American Mineralogist, Volume 101, pages 2085–2094, 2016

Modeling dislocation glide and lattice friction in Mg_2SiO_4 wadsleyite in conditions of the Earth's transition zone

Sebastian Ritterbex[1,*], Philippe Carrez[1], and Patrick Cordier[1]

[1]Unité Materiaux et Transformations, CNRS–UMR 8207, Université Lille 1, 59655 Villeneuve d'Ascq, France

Abstract

Thermally activated dislocation glide in Mg_2SiO_4 wadsleyite at 15 GPa has been modeled to investigate its potential contribution to plastic deformation of wadsleyite in the Earth's transition zone. Modeling is based on a multiphysics approach that allows calculating the constitutive equations associated with single slip for a wide range of temperatures and strain rates typical for the laboratory and the Earth's mantle. The model is based on the core structures of the rate limiting ½<111>{101} and [100](010) dissociated screw dislocations. After quantifying their lattice friction, glide is modeled through an elastic interaction model that allows calculating the critical configurations that trigger elementary displacements of dissociated dislocations. The constitutive relations corresponding to glide are then deduced with Orowan's equation to describe the average intracrystalline plasticity. The high stresses predicted by the model are found to be in good agreement with experimental data on plastic deformation of wadsleyite at high-pressure conditions. Moreover, it is found that even at appropriate mantle strain rates, glide of dislocations remain difficult with critical resolved shear stress (*CRSS*) values typically larger than 100 MPa. This implies the inefficiency of dislocation glide to the overall plastic deformation of Mg_2SiO_4 wadsleyite under transition zone conditions.

Keywords: Wadsleyite, transition zone, plastic deformation, dislocation glide, dissociated dislocations, glide mobility

Introduction

The 410 km seismic discontinuity is widely accepted to be the consequence of the phase transformation of olivine into wadsleyite. The discontinuity is due to the ongoing changes in physical properties between both polymorphs (Goldschmidt 1931; Ringwood and Major 1966; Akimoto and Sato 1968; Irifune and Ringwood 1987). This phase change is likely to influence the convective pattern at the top of the transition zone because mantle flow is controlled by the viscosity of the constituent mantle phases. As $(Mg,Fe)_2SiO_4$ wadsleyite is considered to be the primary phase from 410 to 520 km depth, its rheological properties will determine the solid-state flow in the uppermost part of the mantle transition zone. The rheological contrast between the upper mantle and the top of the transition zone may have implications for the fate of subducting slabs that enter the Earth's transition zone as inferred from seismic tomography (van der Hilst et al. 1997; Grand et al. 1997; Fukao et al. 2001; Fukao and Obayashi 2013). The effect on global mantle convection still remains unsolved (Davies 1995; Bunge et al. 1996, 1997; Bina et al. 2001; Kárason and van der Hilst 2000; Karato et al. 2001; Zhao 2004). Therefore, describing the plastic deformation of wadsleyite is mandatory to gain insight into the convective flow at the boundary between the upper and the lower mantle.

Wadsleyite is a sorosilicate with an orthorhombic crystal structure of space group *Imma*. Previous studies (Dupas et al. 1994; Sharp et al. 1994; Dupas-Bruzek et al. 1998; Thurel 2001; Thurel et al. 2003b; Metsue et al. 2010) suggest that the two easiest slip systems are ½<111>{101} and [100](010). They involve dislocations dissociated into collinear partials. Numerous deformation experiments have been conducted to investigate the plasticity of wadsleyite (Chen et al. 1998; Thurel and Cordier 2003; Thurel et al. 2003a, 2003b; Nishihara et al. 2008; Farla et al. 2015; Hustoft et al. 2013; Kawazoe et al. 2010, 2013). Despite a considerable amount of mechanical data obtained under laboratory conditions, it remains experimentally impossible to derive constitutive equations related to the extremely low-strain rate conditions of the Earth's mantle without the need of extrapolations.

As such, we propose using a computational mineral physics approach to study plastic deformation of wadsleyite at 15 GPa. Regarding plastic deformation, dislocation glide is often considered as one of the most efficient strain producing deformation mechanisms in intracrystalline plasticity. However, in contrast to the latter hypothesis, Ritterbex et al. (2015) show the inefficient contribution of dislocation glide to the overall plasticity of Mg_2SiO_4 ringwoodite under transition zone conditions. Starting from Metsue et al. (2010), who calculated the easiest slip systems and determined the associated dislocation core structures in Mg_2SiO_4 wadsleyite at 15 GPa, the aim of the present work is to determine the glide mobility of these rate-controlling dislocations as a function of stress and temperature. Since the modeling approach of Ritterbex et al. (2015) was based on the mobility of dissociated dislocations, the same methods will be applied to investigate the potential contribution of dislocation

* E-mail: sebastian.ritterbex@ed.univ-lille1.fr

0003-004X/16/0009–2085$05.00/DOI: http://dx.doi.org/10.2138/am-2016-5578CCBYNCND

glide to the plasticity of wadsleyite under the conditions of the upper transition zone.

To move in high-pressure silicates such as wadsleyite, dislocations have to overcome their intrinsic lattice resistance. Plastic slip in this so-called thermally activated regime, is mainly governed by the sluggish glide of long ½<111>{101} and [100](010) screw segments (Metsue et al. 2010). If a dislocation bows out in its glide plane under the conjugate action of stress and thermal activation, it activates non-screw segments that leave behind straight slow-moving screw lines, which in turn will account for most of the plastic strain produced. Based on this mechanism, our model is able to determine the temperature threshold T_a (athermal temperature) below which the glide mobility of dislocations is primarily dominated by lattice resistance as experienced by the rate-controlling screw segments.

The kinematics of thermally activated glide depend strongly on the specific atomic arrangements that build the dislocation cores. The core structures belonging to the easiest ½<111>{101} and [100](010) slip systems, which have been calculated by Metsue et al. (2010), are reevaluated by making use of the Peierls-Nabarro-Galerkin (PNG) method. Lattice friction experienced by dislocations on each slip system is then calculated and described by the Peierls potential and its derivative, the Peierls stress. Here, however the main purpose is to model the glide mobility based on the thermally activated motion of the rate-controlling dislocation character of the easiest slip systems over the Peierls barriers by nucleation and propagation of unstable kink-pairs. This can be described through an elastic interaction model, initially proposed by Koizumi et al. (1993). This model has been extended to dissociated dislocations and successfully applied to Mg_2SiO_4 ringwoodite by Ritterbex et al. (2015). It is adopted in the present work to handle kink-pair formation on dissociated dislocations as they occur in wadsleyite. Dislocation mobilities are finally determined from the stress dependence on the nucleation rate of kink-pairs. Single slip constitutive equations describing the temperature dependency on the critical resolved shear stress (*CRSS*), will be derived by solving Orowan's equation as a function of steady-state strain rate. This will be compared to recent data of experimentally deformed wadsleyite. The results enable us to address the role of lattice friction on the dislocation mobility in wadsleyite under pressure and temperature conditions of the upper transition zone. The outcome will be compared to what has been inferred for dislocation glide in Mg_2SiO_4 ringwoodite by Ritterbex et al. (2015). Finally, implications for the rheology of transition zone will be discussed.

Multiscale modeling

Parallell to Ritterbex et al. (2015), our numerical multiscale model relies on two main steps. First, determining the lattice friction experienced by dislocations that belong to the easiest slip systems. This is calculated in the framework of the Peierls-Nabarro (PN) model (Peierls 1940; Nabarro 1947). Second, the elastic interaction model used in Ritterbex et al. (2015) will be applied to calculate the enthalpy variations related to critical configurations that trigger elementary displacements of the rate controlling dissociated dislocations in wadsleyite. Finally, dislocation glide will be described through single slip mobilities, which are deduced from the latter results.

Dislocation core structures and lattice friction

The element free Galerkin method based PNG model (Denoual 2007) has been used by Metsue al. (2010) to model dislocations belonging to the easiest slip systems: ½<111>{101} and [100](010). The calculations rely on the γ-surfaces of the potential slip planes that takes into account the effect of pressure on atomic bonding.

Here the main interest is to quantify the lattice friction of the easiest dislocations by calculating the Peierls potential. This is computed in the framework of the PN model, by making use of the disregistry u_m and of the γ-surfaces (Ritterbex et al. 2015). The disregistry $u_m = u_m^a - u_m^b$ refers to the relative displacement between two misfit half planes *a* and *b*, as the material is decomposed into two elastic half crystals *A* and *B*. The Peierls potential V_p (Eq. 1) can now be obtained by the addition of the following two energy contributions: (1) summation of the non-elastic misfit energy between *m* pairs of crystal planes:

$$V_m = \sum_{m=-\infty}^{m=+\infty} \gamma(u_m) a'$$

(Christian and Vítek 1970; Joós et al. 1994), and (2) summation of the elastic strain energy:

$$V_e = 1/2 \cdot a' \cdot \left\{ \sum_{m=-\infty}^{m=+\infty} \left[\partial\gamma / \partial u_m(u_m) \right]^a \cdot u_m^a + \sum_{m=-\infty}^{m=+\infty} \left[\partial\gamma / \partial u_m(u_m) \right]^b \cdot u_m^b \right\}$$

(Wang 2006). The previous expressions stand for moving the core structure over the Peierls periodicity a' from one to the next stable position in the crystal lattice.

$$V_p = V_m + V_e \tag{1}$$

The Peierls stress can now be given by $\tau_p = \max\{\Sigma\}$, where $\Sigma = b^{-1}\nabla V_p$ corresponds to the Peierls force with *b* being the modulus of the Burgers vector. The Peierls stress can be seen as a pure mechanical measure of the lattice friction and can equally be understood as the *CRSS* at 0 K.

Kink-pair formation on dissociated dislocations

The same approach as in Ritterbex et al. (2015) is used to calculate the saddle point energies ΔH^{crit} of ΔH required to nucleate a bulge from the initial dissociated dislocation lines bowing out over the Peierls potential V_p. This is considered to be the controlling step of thermally activated motion of dislocations in high-lattice friction materials (Kubin 2013). In the presence of low and intermediate stresses, the widths of the complete bulges, which are known as kink-pairs, are much larger than the spread of the individual kinks along the dislocation line (Koizumi et al. 1994). Therefore the model relies on the assumption of displacing elementary segments of width *w* on the initial dislocation line by the nucleation of rectangular kink-pairs of height *h* (Fig. 1). The enthalpy variation ΔH that describes kink-pair formation on dissociated dislocations can be formulated as follows:

$$\Delta H = \Delta E_{\text{elastic}} + c_i \Delta P_p + \Delta W_{sf} + c_i W_p. \tag{2}$$

Equation 2 shows the dependency of the kink-pair formation enthalpy ΔH on the total variation in elastic energy $\Delta E_{\text{elastic}}$, the change in Peierls energy ΔP_p, and the variation in stacking fault

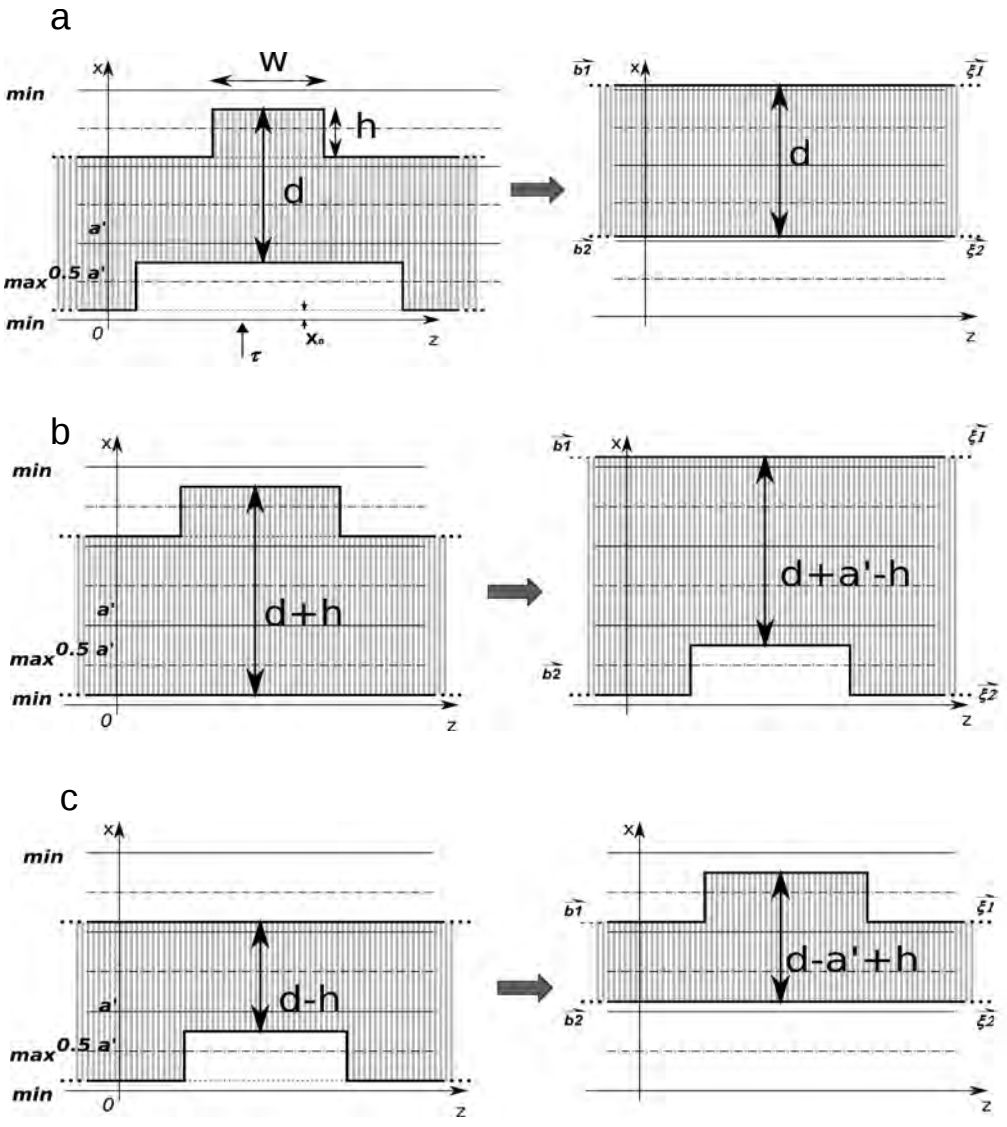

Figure 1. Kink-pair nucleation on collinear dissociated dislocations with equilibrium stacking fault width *d*. (**a**) Correlated nucleation process: coherently simultaneous kink-pair nucleation on partial dislocations. (**b**) Uncorrelated nucleation: kink-pair nucleation starting from the leading partial followed by a nucleation of the trailing partial. (**c**) Uncorrelated nucleation: kink-pair nucleation starting from the trailing partial followed by the nucleation of the leading partial.

energy ΔW_{sf}. The work W_p performed by the resolved shear stress τ on a partial dislocation is given by $-\tau b_p h w$ with b_p equal to the modulus of the partial Burgers vector. The model is based on the necessity to form a kink-pair on both partials to move the complete dislocation. This can occur either through "correlated" nucleation of kink-pairs along both partials or through independent nucleation that starts on one and is followed by the formation of a kink-pair on the other partial. As such, it has been taken into account that each equivalent partial has to overcome half of the complete Peierls potential V_p (Eq. 1). The constants c_i in Equation 2 refer to $c_i = c_u = 1$ for uncorrelated and $c_i = c_c = 2$ for correlated kink-pair nucleation. The critical nucleation enthalpy ΔH^{crit} can thus be found as the saddle point configuration of $\Delta H(w,h)$ as a function of the resolved shear stress τ.

Figure 1 shows the characteristics of kink-pair nucleation on collinear dissociated dislocations under the action of a resolved shear stress. Starting from Figure 1a at low-stress conditions, kink-pair nucleation is forced to occur in a correlated manner on both partials, since the work done by the stress cannot overcome the increase in absolute energy related to substantial changes in the equilibrium stacking fault width *d* inherent to uncorrelated nucleation (Möller 1978; Takeuchi 1995; Mitchell et al. 2003). Only small local variations of the stacking fault are allowed. The small variations in *d*, in case of low-energy stacking fault systems (e.g., partials separated by a large equilibrium distance *d*), are able to reduce the saddle point configuration of the metastable system by lowering the stacking fault energy without any change in elastic interaction between the partials. Under these low-stress

conditions, the widths w_1 (partial 1) and w_2 (partial 2) between the kink-pairs are relatively equal. However, if stress increases, one of the kink-pairs tend to collapse and the kink-pair nucleation process becomes gradually decoupled: independent uncorrelated kink-pair nucleation on both partials become favorable (Figs. 1b and 1c). This implies that uncorrelated nucleation of kink-pairs can only occur and is favorable at $\tau \geq \tau_c$, where τ_c is equal to a critical stress. See supplementary material[1] and Ritterbex et al. (2015) for a detailed description of the kink-pair model.

Results

Dislocation cores and their lattice friction

The dislocation core structures belonging to the easiest ½<111>{101} and [100](010) slip systems have been calculated by Metsue et al. (2010) using the PNG method. Calculations relied on the γ-surfaces of the potential slip planes. Metsue et al. (2010) shows that dislocation core structures of both slip systems are more confined for the screw than for the edge dislocations. As a consequence, lattice friction will be lower for the edge than for the screw dislocations. As the edge characters exhibit lower lattice friction, the mobility of the ½<111>{101} and the [100](010) screw dislocations will account for most of the plastic strain produced during deformation since the amount contributed by the faster edge segments is negligible. We have reevaluated the core structures of the ½<111>{101} and [100](010) screw dislocations following Metsue et al. (2010). The resulting dislocation core structures are shown in Figure 2 by the disregistry and its derivative, the local Burgers vector density. This shows the dissociation of both screw dislocations into two collinear partials. The Burgers vector reaction for the ½<111> screw in the {101} plane is ½<111> = ⅖<111> + ⅗<111>. The Burgers vector reaction for the [100] screw in the (010) plane is [100] = ½[100] + ½[100]. It is worth to mention that the equilibrium stacking fault width d (see Fig. 2) between the partials is always found to be equal to an integer multiple of the Peierls periodicity a'. This means that both partials occupy the minimum energy configuration in the crystal system under equilibrium conditions, so that both partials are well placed into the wells of the Peierls potential.

The Peierls potentials are derived according to Equation 1 and Peierls stresses are evaluated by the maximum derivative of the Peierls potentials. Tables 1 and 2 show the properties related to the dislocation core structures and Peierls stresses for both slip systems, respectively. Peierls potentials and their derivatives are shown in Figure 3. Both slip systems have a value of $\tau_p/\mu \sim 3.5 \times 10^{-2}$. A value of $\tau_p/\mu \sim 5 \times 10^{-2}$ has been found in Mg_2SiO_4 ringwoodite (Ritterbex et al. 2015) with respect to the rate controlling dislocations of the easiest slip systems. A comparison with $\tau_p/\mu \sim 1 \times 10^{-2}$ in MgO (Amodeo et al. 2011) at similar pressure conditions indicates higher lattice friction in both high-pressure polymorphs of olivine.

Thermal activation of glide: Kink-pair mechanism

Critical enthalpies associated with kink-pair nucleation are calculated in the framework of the elastic interaction model as adapted to dissociated dislocations (Ritterbex et al. 2015). Based on linear elasticity, the shear modulus μ and the Poisson ratio ν at 15 GPa have been deduced using the DisDi sofware (Douin 1987). As the latter relies on Stroh theory, the anisotropic elastic parameter $K(\theta)$ for the screw character is given by $K(0°) = \mu$ and for the edge character by $K(90°) = \mu/(1 - \nu)$. Finally, the core structures (Fig. 2; Table 1) of the ½<111>{101} and the [100](010) screw dislocations and the quantification of their intrinsic lattice friction (Fig. 3; Table 2) are used to calculate the critical nucleation enthalpies ΔH^{crit}.

Kink-pair nucleation on the ½<111>{101} screw dislocation can be described as in the general case for dissociated dislocations as already discussed in Ritterbex et al. (2015). This means that correlated nucleation of kink-pairs is captured by the single critical activation enthalpy ΔH_c^{crit}. Uncorrelated kink-pair nucleation is essentially determined by the outward motion of the leading partial associated with the nucleation process as shown in Figure 1c, which is captured by the critical activation enthalpy ΔH_u^{crit}.

This is not the case for the [100](010) screw dislocation since the equilibrium dissociation width d is equal to a single period a' of the Peierls potential (Table 1): kink-pair nucleation that

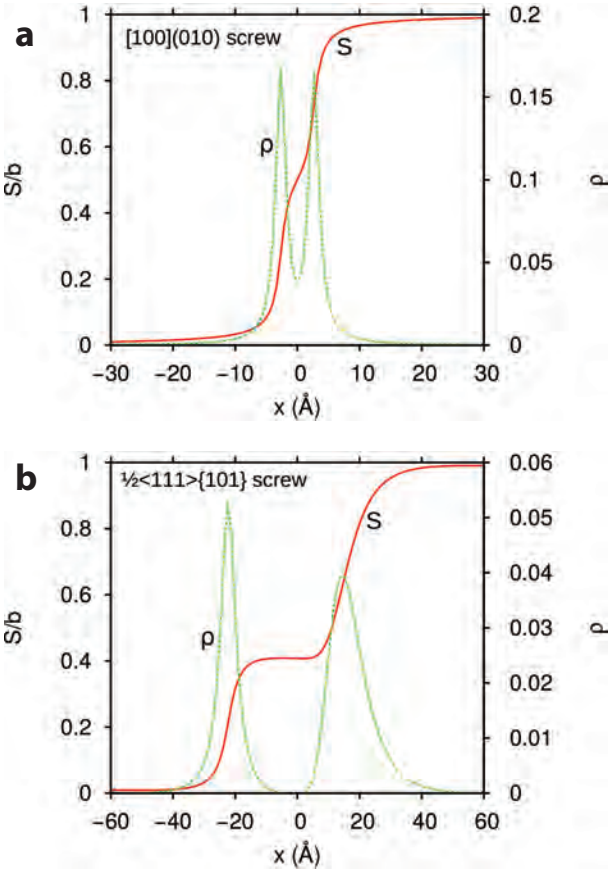

Figure 2. Results of the PNG calculations in form of the disregistry (red continuous line) and its derivative, the local density of the Burgers vector (green dotted line) of the: (**a**) [100](010) screw dislocations and (**b**) ½<111>{101} screw dislocations.

[1]Deposit item AM-16-95578, Supplemental Material. Deposit items are free to all readers and found on the MSA web site, via the specific issue's Table of Contents (go to http://www.minsocam.org/MSA/AmMin/TOC/).

starts form the trailing partial is not possible. The evolution of the critical nucleation enthalpy with resolved shear stress for this slip system is therefore entirely given by ΔH_c^{crit} (Fig. 4), since the uncorrelated nucleation process as shown in Figure 1b is completely governed by the critical enthalpy $\Delta H_{u,l1}^{crit} \approx \Delta H_c^{crit}$, associated with the outward motion of the leading partial.

TABLE 1. Core structures of the ½<111>{101} and [100](010) screw dislocations with Peierls periodicity a'

Dislocation	b_p (Å)	$K(\theta = 0°)$ (GPa)	$K(\theta = 90°)$ (GPa)	a' (Å)	ξ (Å)	d (Å)
[100](010)	2.803	123	185	4.028	2.0	5.4
½<111>{101}	$b_{p1} = 2.987$	128	171	7.3	$\xi_1 = 8.4$	35.8
	$b_{p2} = 4.480$				$\xi_2 = 12.5$	

Notes: $K(\theta)$ is equal to the anisotropic elastic parameter, ξ corresponds to the width of each partial, d is equal to the equilibrium stacking fault width taken as the distance between the partials, and τ_p corresponds to the Peierls stress.

TABLE 2. Key features and parameterization related to the glide as a result of correlated kink-pair nucleation of the governing screw dislocations

Dislocation	τ_p (GPa)	ΔH_0 (eV)	p	q
[100](010)	4.8	12.5	0.5	1.03
½<111>{101}	3.5	12.3	0.5	1.61

Notes: ΔH_0 is the critical nucleation enthalpy at $\tau = 0$, a' the Peierls periodicity, τ_p corresponds to the Peierls stress, and p and q are together with ΔH_0 the empirical fitting parameters of Equation 5.

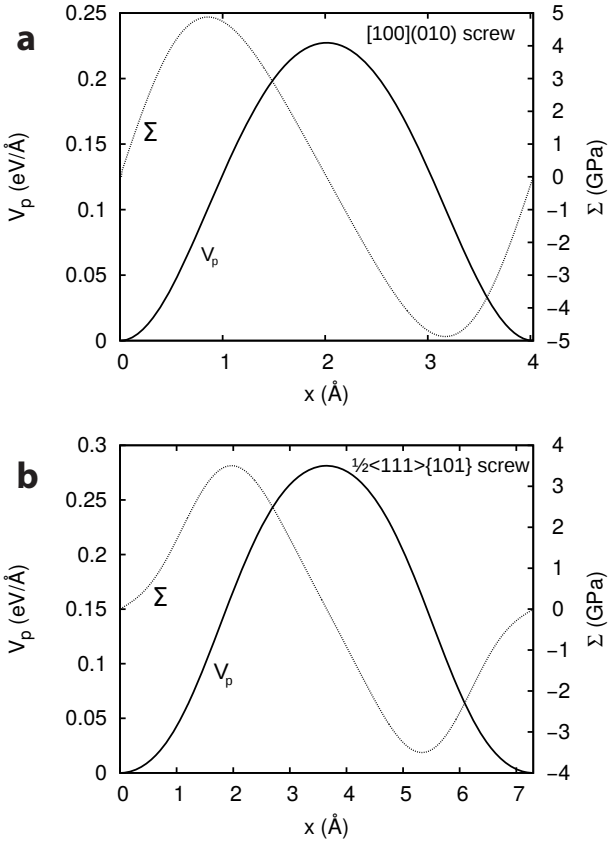

FIGURE 3. Peierls potentials $V(p)$ and subsequent Peierls force $\Sigma = b^{-1}\nabla V_p$ calculated in the framework of the PN model and based on the dislocation structures for the (**a**) [100](010) screw and (**b**) ½<111>{101} screw dislocations. The potentials give a pure mechanical measure of the lattice friction of both slip systems. The latter will serve as input to calculate the thermally activated mobility of the respective screw dislocations.

The elastic interaction model is restricted to the low and intermediate stress regime (Caillard and Martin 2003). However, the critical nucleation enthalpies can be extrapolated up to the Peierls stress using the classical formalism of Kocks et al. (1975):

$$\Delta H^{crit}(\tau) = \Delta H_0[1 - (\tau_{eff}/\tau_p)^p]^q \quad (3)$$

where ΔH_0 is equal to $\Delta H_c^{crit}(\tau = 0)$ and $\Delta H_u^{crit}(\tau = \tau_c)$ for the correlated and uncorrelated kink-pair nucleation mechanims, respectively. τ_{eff} is defined as the effective resolved shear stress. For correlated nucleation $\tau_{eff} = \tau$ and for uncorrelated nucleation $\tau_{eff} = \alpha(\tau - \tau_c)$, with $\alpha = \tau_p/(\tau_p - \tau_c) \approx 1$, where τ_c is equal to the critical resolved shear stress above which uncorrelated nucleation is able to occur (Table 3). The empirical parameters p and q are obtained from a least-square minimization between the Kocks formalism (Eq. 3) and the evolution of $\Delta H^{crit}(\tau)$ of kink-pair nucleation as calculated with the elastic interaction model. Results of the critical nucleation enthalpies as a function of resolved shear stress for both slip systems are presented in Figure 4.

Dislocation mobility

The dislocation velocity depends on the waiting time for a kink-pair nucleation process to occur at both partials under the action of applied resolved shear stress and thermal activation. This waiting time can be expressed in terms of the rate of kink-

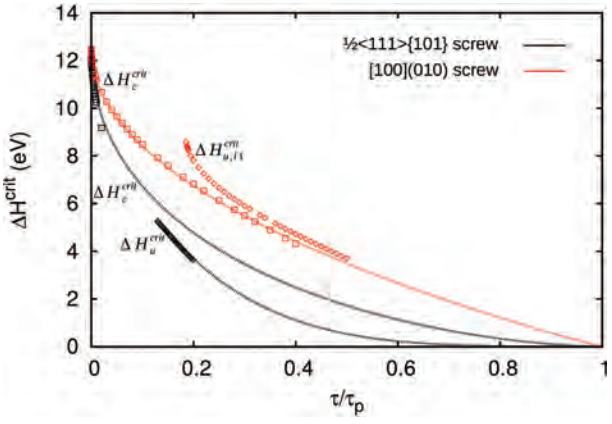

FIGURE 4. Evolution of the critical kink-pair nucleation enthalpy as a function of the resolved shear stress (normalized by the Peierls stress) for the [100](010) screw and the ½<111>{101} screw dislocations. Results are shown for correlated nucleation and the relevant elementary steps of the uncorrelated nucleation processes.

TABLE 3. Key features and parameterization related to the glide as a result of uncorrelated kink-pair nucleation of ½<111>{101} screw dislocation, where ΔH_0 is the critical nucleation enthalpy at $\tau = \tau_c$

Dislocation	τ_p (GPa)	τ_c (GPa)	ΔH_0 (eV)	p	q
[100](010)	4.8	0.89	8.6	n/a	n/a
½<111>{101}	3.5	0.455	5.3	1.0	5.0

Notes: The remaining parameters are defined as in Table 2. The uncorrelated kink-pair nucleation of the [100](010) screw dislocations can be described as in Table 2 since it is constrained to kink-pair nucleation starting at the leading partial.

pair nucleation J. The dislocation velocity is given by Equation 4, where a' (Peierls periodicity) is the unit distance to move a complete (dissociated) dislocation.

$$V(\tau,T) = a'J \tag{4}$$

The rate of kink-pair nucleation J (Dorn and Rajnak 1964; Guyot and Dorn 1967; Möller 1978) is given by

$$J = \nu_0 \frac{b_p}{w^{\text{crit}}(\tau)} \frac{L}{c_i b_p} \exp\left(-\frac{\Delta H^{\text{crit}}(\tau)}{k_b T}\right) \tag{5}$$

where b_p is the modulus of the Burgers vector of the partials, w^{crit} is the critical width between kink-pairs, ν_0 is equal to the Debye frequency, k_b is the Boltzmann constant, and T is the temperature. The pre-exponential factor on the right side of Equation 5 is composed of two contributions of which the first one is equal to the vibration frequency $\nu_0 b_p/w^{\text{crit}}$ of the partial segments where nucleation initiates. The second contribution is the number of potential activation sites $L/c_i b_p$, taking into account that only the resonance modes allow correlated nucleation on both partials to occur. The average length L of the dislocation segments can be expressed in terms of the dislocation density ρ_m as $L = 1/\sqrt{\rho_m}$. The dislocation density ρ_m is taken to be $10^{12} m^{-2}$ under experimental and $10^8 m^{-2}$ under mantle conditions to take into account the stress differences between both regimes.

Following Möller (1978), the average dislocation mobility can now be formulated as:

$$V(\tau,T) = \tfrac{1}{2}\, a'(J_c + J^*) \tag{6}$$

where J_c corresponds to the rate of correlated kink-pair nucleation (Eq. 5). If $\tau < \tau_c \rightarrow J^* = J_c$ and if $\tau \geq \tau_c \rightarrow J^* = J_u$ where J_u corresponds to the nucleation rate associated with uncorrelated kink-pair nucleation (Eq. 5).

Dislocation velocity profiles $V(\tau)$ at fixed temperatures for both ½<111>{101} and [100](010) screw dislocations are shown in Figure 5. The critical shear stress τ_c below which only correlated kink-pair nucleation can occur is equal to about 500 and 900 MPa for the ½<111>{101} screw and [100](010) screw dislocations, respectively (Table 3). Figure 5a shows the resolved shear stress dependence of the velocities for both screw dislocations at 1700 K in a log-log plot. This clearly shows that the velocity of the ½<111>{101} screws, independent of the applied stress, is always larger than that of the [100](010) screw dislocations. The small window in Figure 5a shows the same velocity curves in a semi-log plot, which gives a better insight into the velocity differences with stress between both screw dislocations. Here, we can observe that at high, but mainly at intermediate stress values, the velocity differences between both slip systems are relatively large and decrease with decreasing stress. At very low-stress levels (what can be expected in mantle conditions), the dislocation velocities for both screws become more comparable. Typical laboratory strain rates of $\dot{\varepsilon} = 10^{-5} s^{-1}$ correspond to dislocation velocities of about $V = 2 \times 10^{-8}$ m/s. The stresses associated with these velocities are in the order of 0.5–2 GPa. In contrast, dislocation velocities related to mantle strain rates of $\dot{\varepsilon} = 10^{-16}\ s^{-1}$ are about $V = 2 \times 10^{-15}$ m/s with stresses of ~200–1000 MPa. At room temperature, the velocity

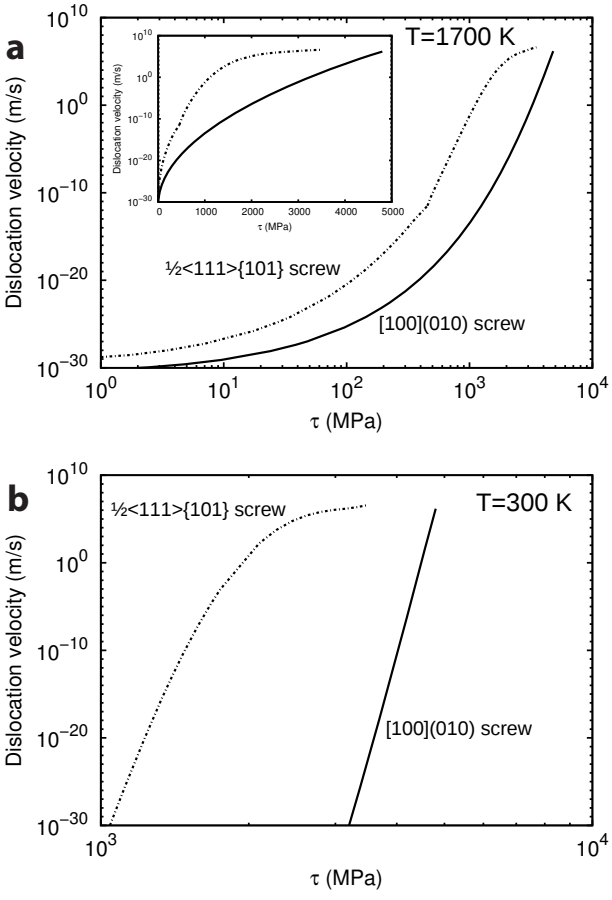

Figure 5. Glide velocity of the ½<111>{101} and [100](010) screw dislocations as a function of the resolved shear stress at: (**a**) 1700 K and (**b**) 300 K.

evolution with stress of the same screw dislocations are shown in Figure 5b. Here, physically relevant dislocation glide only takes place in the high-stress regime where uncorrelated nucleation of kink-pairs govern the dislocation mobility. The overall trend of the velocity profiles at room temperature are comparable to the results at 1700 K. Stresses of about 1–4 GPa are required to obtain dislocation velocities corresponding to typical laboratory strain rates at room temperature. Finally, one can observe that the dislocation velocities at the Peierls stress for each individual dislocation are strictly independent of temperature since this stress corresponds to the resolved shear stress required to move an infinite dislocation at the absolute zero. At the Peierls stress, the mobility of dislocations is governed by other mechanisms than the nucleation of kink-pairs and the results of $\lim_{\tau \rightarrow \tau_p} V(\tau)$ are considered to be unphysical.

Discussion

General discussion

In 2010, Metsue et al. already modeled the core structures of dislocations in wadsleyite using the PNG model. Here, the core structures of the rate controlling ½<111>{101} and [100](010) screw dislocations are recalculated using the same approach,

showing a good agreement with results previously obtained by Metsue et al. (2010). Lattice friction of these screw dislocations are quantified by explicit calculation of the Peierls potentials within the framework of the PN model. The Peierls stresses calculated in this study are about one order of magnitude larger than the ones of Metsue et al. (2010). However, the relative differences between both screw dislocations are found to be equal. Nevertheless, the values of τ_p obtained in this study are more in line with what can be expected from experiments (Nishihara et al. 2008; Kawazoe et al. 2013; Hustoft et al. 2013; Farla et al. 2015).

We show that the Burgers vector reaction for the [100] screw dislocation in the (010) plane corresponds to [100] = ½[100] + ½ [100]. This dissociation is collinear and both partials are strictly equivalent. The collinear partials of the ½<111> screw dislocation in the {101} plane with Burgers vector reaction: ½<111> = ⅖<111> + ⅗<111> are not equivalent. However, the asymmetry between the partials is small and is neglected throughout the calculations of the dislocation mobility. As a matter of fact, the core structure of this dislocation is widely spread with a large equilibrium stacking fault width (d = 35.8 Å) (Fig. 2b). This significant core extension is confirmed by clear weak-beam dark-field observation of both partials of the ½<111>{101} dislocation using transmission electron microscopy (TEM) (Thurel and Cordier 2003). The effect of this low-energy stacking fault on the mobility is more important than the small difference between both partials. So formally, we assume both partials of the ½<111> dislocation to be equal to ¼<111>.

In the second part of the work, dislocation mobilities related to single slip systems are calculated. Dislocation velocities are obtained by using the elastic interaction model, based on the thermal activation of glide of dissociated dislocations (Ritterbex et al. 2015). Figure 5a clearly shows a pronounced difference in the evolution of $V(\tau)$ at 1700 K for both screw dislocations considered. This difference is directly related to the difference in evolution of $\Delta H^{crit}(\tau)$ (Fig. 4). The latter, once more, is the consequence of the different core structures between the [100](010) and ½<111>{101} screw dislocations: [100](010) exhibits narrow dissociation with a confined spreading of the partials, whether ½<111>{101} is characterized by an extended dissociation with a wide spread of the partials (Fig. 2). These features finally determine the velocity evolution $V(\tau)$ of the dislocations. The results further show that correlated nucleation of kink-pairs, which coincide along both partials is possible at every stress, whereas uncorrelated nucleation is only possible and becomes more favorable than correlated nucleation at $\tau \geq \tau_p$ due to lower critical nucleation enthalpies. This implies that dislocation glide operating by the Peierls mechanism at low temperatures and high-deviatoric stress (in most cases, laboratory conditions), will be mainly governed by uncorrelated nucleation of kink-pairs. However, at high temperatures and small deviatoric stresses (more likely to represent mantle conditions), glide will be predominantly controlled by correlated nucleation of kink-pairs on both partials.

Steady-state plastic flow as a consequence of single slip can now be formulated by relating the glide mobility $\nu(\tau,T)$ to the macroscopic strain rate $\dot{\varepsilon}$ by the use of Orowan's equation: $\dot{\varepsilon} = \rho_m b V(\tau,T)$, where ρ_m corresponds to the mobile dislocation density and b equals the modulus of the complete Burgers vector for each respective slip system.

Deformation under laboratory conditions

To compare the results of our model with mechanical data available from high *P-T* experiments, we solve Orowan's equation as function of strain rate $\dot{\varepsilon}$ for which the resolved shear stress τ can then be seen as the *CRSS*. We have calculated the *CRSS* over a broad range of temperatures for a typical laboratory strain rate of $\dot{\varepsilon} = 10^{-5}s^{-1}$. Figure 6 shows the results for the slip of the rate governing ½<111>{101} and [100](010) screw dislocations. The transition of the curves to the dotted lines at 2500 K marks the onset to melting for the Mg_2SiO_4 system around 15 GPa. This demonstrates that dislocation glide in wadsleyite at laboratory strain rates always operates in the thermally activated regime, since the athermal temperature would be higher than the melting temperature. It means that intracrystalline plasticity under laboratory conditions is mainly governed by the mobility of the rate controlling slip systems. The results show that slip of the ½<111>{101} screws is always easier than slip of the [100](010) screw dislocations for the whole stress range $0 < CRSS \leq \tau_p$. Furthermore, one can observe that the evolution of the $CRSS(T)$ for both screw dislocations is significantly different. This is directly related to the difference in core structure between both screw dislocations and the subsequent difference in equilibrium stacking fault energies. Whereas the evolution at high *CRSS* and low T for [100](010) screws is roughly linear, the same evolution for the ½<111>{101} screw dislocations is highly exponential. At high T where both curves converge toward each other, the difference in $CRSS(T)$ are found to be the smallest. Figure 6 shows a remarkably good agreement between our theoretical predictions and the experimental data available. It is worth to mention that the deformation experiments used (Nishihara et al. 2008; Kawazoe et al. 2010, 2013; Hustoft et al. 2013; Farla et al. 2015) were performed on polycrystalline wadsleyite samples. The raw experimental data instead display the temperature dependence on the effective flow stress rather than on the *CRSS* related to single slip systems as in our calculations.

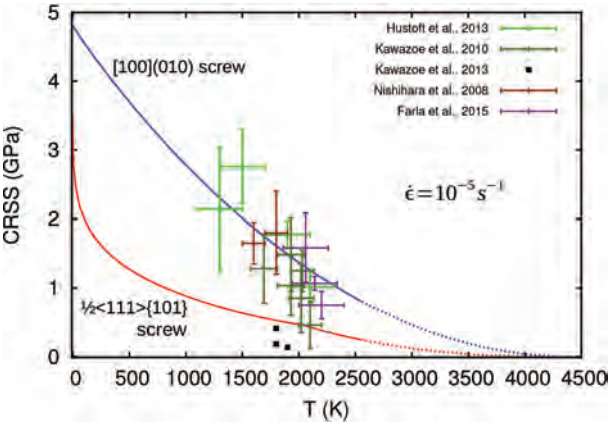

Figure 6. Constitutive relation shown as the *CRSS* vs. temperature at a fixed strain rate of $\dot{\varepsilon} = 10^{-5}s^{-1}$ for thermally actived glide of the rate controlling ½<111>{101} and [100](010) screw dislocations. The mobile dislocation density is taken to be $\rho_m = 10^{12}m^{-2}$. The experimental effective flow stresses are divided by two (corresponding to the maximum of the Schmid factor) to be converted into apparent resolved shear stresses since deformation experiments were performed on polycrystalline samples.

Only a fraction of the effective flow stress is resolved in the slip direction within each single slip plane. As such, the experimental data are divided by two (corresponding to the maximum of the Schmid factor) to be compared with our resolved shear stresses in Figure 6. The latter assumption may be too simple as more deformation mechanisms may be involved in the experiments and effects of impurities and hardening due to texture formation has not been taken into account in our model. However, a posteriori TEM observations of deformed samples in some of the experimental studies (e.g., Hustoft et al. 2013; Farla et al. 2015) clearly reveal the potential contribution of dislocation glide to the overall deformation under laboratory conditions by the development of dense microstructures with high-dislocation densities ($>10^{12}m^{-2}$). Furthermore, the agreement between the experimental data and the evolution of the *CRSS* with *T* of the rate controlling dislocations shows that glide controls largely the mechanical behavior in laboratory conditions.

Deformation under transition zone conditions

Strain rate is one of the important physical conditions that determine the potential contribution of a deformation mechanism to the overall plasticity. Unfortunately, there is a large discrepancy between the very low-strain rates at which the high-pressure silicates of the Earth's mantle deform and the laboratory conditions, which correspond to strain rates of about $10^{-5}s^{-1}$. Experimental constitutive equations therefore have to rely on the extrapolation down to typical mantle strain rates of $10^{-16}s^{-1}$. However, the extrapolation cannot account for the intrinsic strain rate dependency on the mobility of the defects.

By modeling the glide mobility of the rate controlling dislocations, we are able to calculate the evolution of *CRSS*(*T*) for typical mantle strain rates $\dot{\varepsilon} = 10^{-16}s^{-1}$ without the need of extrapolation. Modeling of the glide plasticity has been performed at 15 GPa, since wadsleyite is stable in the upper half of the transition zone, from 410–520 km at a pressure range of 13–18 GPa, which corresponds to a temperature interval around 1700 K. Results of the evolution of the *CRSS*(*T*) are shown in Figure 7. One can observe that the minimum *CRSS* lies around 200 MPa for the easiest slip system up to over 600 MPa for the more difficult slip system at 1700 K. The results show that glide in wadsleyite under mantle conditions still occurs in a regime where the *CRSS* is temperature dependent (thermally activated regime). This implies that plastic deformation by dislocation glide in wadsleyite under conditions of the upper transition zone is governed by the average mobility of the rate governing screw dislocations. However, it has to be mentioned that the temperature dependency of the *CRSS* is a function of the applied strain rate and the mobile dislocation density.

Finally, it follows from our study that the relative ease of glide of the different slip systems, as derived by the intrinsic lattice friction and defined by the Peierls stress, is not affected by temperature and strain rate, since glide of the ½<111>{101} remains easier than [100](010) glide in the whole range of conditions considered. Together with the fact that ½<111>{101} has more symmetrical variants than [100](010), we estimate that ½<111>{101} slip will play a dominant role in dislocation glide governed deformation of (poly)crystalline wadsleyite under both natural and laboratory conditions.

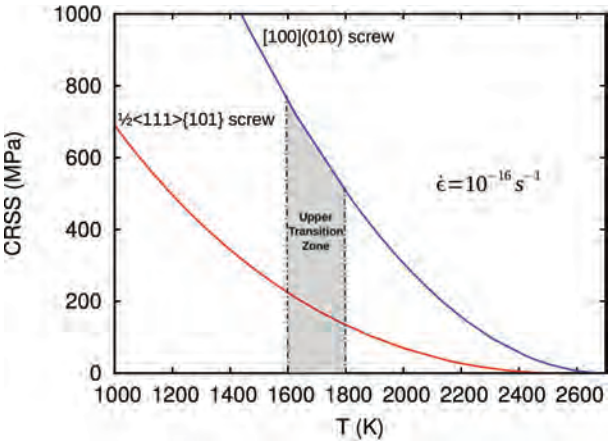

Figure 7. Constitutive relations shown as the *CRSS* vs. temperature at a fixed strain rate of $\dot{\varepsilon} = 10^{-16}s^{-1}$ for thermally actived glide of the rate controlling ½<111>{101} and [100](010) screw dislocations. The dislocation density is taken to $\rho_m = 10^8m^{-2}$ to adjust to the low-stress regime in the Earth's mantle. The shaded area depicts the stability field of wadsleyite in the upper transition zone at 15 GPa.

Implications

The above results show the inefficiency of dislocation glide as a strain producing deformation mechanism under transition zone conditions. To compare the wadsleyite results to glide in ringwoodite, we calculate the viscosities η associated with single slip as $\eta = CRSS(T = 1700\text{ K})/2\dot{\varepsilon}$. A viscosity between (0.9–3) $\times 10^{24}$ Pa·s can be attributed to slip of the ½<111>{101} and [100](010), respectively. Similar single slip viscosities in the order of 10^{24} Pa·s were found for Mg_2SiO_4 ringwoodite (Ritterbex et al. 2015) deforming by dislocation glide. As for comparison, a viscosity at transition zone depth in the order of 10^{21}–10^{22} Pa·s may be expected from global joint inversion (Mitrovica and Forte 2004). This shows that the sole contribution of dislocation glide is unlikely to account for the overall plasticity of Mg_2SiO_4 wadsleyite and ringwoodite under transition zone conditions. It is essentially the evolution of the critical kink-pair nucleation enthalpies $\Delta H^{crit}(\tau)$ that determine the constitutive equations as shown is Figures 6 and 7. Typical values of the critical nucleation enthalpies at low-stress conditions of the mantle for the rate controlling dislocations in both high-pressure polymorphs of olivine are found to be $\lim_{\tau \to 0} \Delta H^{crit} > 10$ eV. This is what makes glide difficult to activate.

High values of the *CRSS*(*T*) regarding pure single slip dislocation glide suggest that other mechanisms may control the deformation of wadsleyite and ringwoodite in the Earth's transition zone. In fact, the transition zone is characterized by several phase transformations, which may give rise to transformation plasticity, sometimes referred to as transformational superplasticity. The phase transformations, furthermore are often accompanied by grain size reduction, which may enhance diffusion mechanisms as is the same for water weakening processes due to the water bearing capacity of wadsleyite and ringwoodite (Chen et al. 1998; Huang et al. 2005). Finally, significant lattice friction that is opposed to glide may also activate climb-controlled diffusion-based intracrystalline deformation.

Nevertheless, some studies report about the local stagnation of slabs where subducting lithosphere deflects laterally just above or within the Earth's transition zone (van der Hilst et al. 1991, 1997; Tajima and Grand 1995; Fukao et al. 2001; Grand 2002; Zhao 2004; Fukao and Obayashi 2013). Local slab stagnation in the transition zone may therefore be related to high-lattice resistance associated with plastic slip in both wadsleyite and ringwoodite, whereas it is expected that more efficient deformation mechanisms other than dislocation glide have to be responsible for the overall plasticity of both high-pressure polymorphs of olivine in the Earth's transition zone. This must at least be the case where slabs penetrate unhindered into the lower mantle.

Concluding remarks

Dislocation glide in Mg_2SiO_4 wadsleyite has been modeled at 15 GPa under laboratory and natural conditions. The model relies on the core structures of the rate governing ½<111>{101} and [100](010) screw dislocations. A crucial feature of these screw dislocations is the collinear dissociation into partials, which determines their mobility. Intrinsic resistance of the crystal lattice that is opposed to glide has been calculated and used to model thermal activation of these dissociated dislocations to calculate the respective glide velocities. Plastic deformation by dislocation glide is finally presented as the response of the temperature dependency of the *CRSS* to an applied strain rate at steady-state conditions. A good agreement between our results at typical laboratory strain rates of $\dot{\varepsilon} = 10^{-5}s^{-1}$ and experimental data on plastic deformation of wadsleyite demonstrates that dislocation glide controls largely the mechanical behavior at laboratory conditions. This validation allows to calculate the constitutive equations related to dislocation glide for typical mantle strain rates of $\dot{\varepsilon} = 10^{-16}s^{-1}$. It is clear that lattice friction in wadsleyite cannot be neglected at those low-strain rates in a similar way as in Mg_2SiO_4 ringwoodite that has already been studied. This indicates the inefficiency of dislocation glide as a strain producing deformation mechanism under transition zone conditions. The results suggest that dislocation glide is not an efficient deformation mechanism to operate in natural conditions for both high-pressure polymorphs of olivine. This implies the necessity of deformation mechanisms other than dislocation glide to be responsible for the overall plasticity of wadsleyite and ringwoodite in the Earth's transition zone.

Acknowledgments

This work was supported by funding from the European Research Council under the Seventh Framework Programme (FP7), ERC Grant No. 290424, RheoMan.

References cited

Akimoto, S., and Sato, Y. (1968) High pressure transformation in Co_2SiO_4 olivine and some geophysical implications. Physics of the Earth and Planetary Interiors, 1, 498–504.

Amodeo, J., Carrez, Ph., Devincre, B., and Cordier, P. (2011) Multiscale modelling of MgO plasticity. Acta Materialia, 59, 2291–2301.

Bina, C.R., Stein, S., Marton, F.C., and Van Ark, E.M. (2001) Implications of slab mineralogy for subduction dynamics. Physics of the Earth and Planetary Interiors, 127, 51–66.

Bunge, H.-P., Richards, M.A., and Baumgardner, J.R. (1996) Effect of depth-dependent viscosity on the planform of mantle convection. Nature, 379, 436–438.

——— (1997) A sensitivity study of three-dimensional spherical mantle convection at 10^8 Rayleigh number: Effects of depth-dependent viscosity, heating mode, and an endothermic phase change. Journal of Geophysical Research, 102, 11991–12007.

Caillard, D., and Martin, J.L. (2003) Thermally Activated Mechanisms in Crystal Plasticity. Pergamon Materials Series, Amsterdam.

Chen, J., Inoue, T., Weidner, D.J., Wu, Y., and Vaughan, M.T. (1998) Strength and water weakening of mantle minerals, olivine, wadsleyite and ringwoodite. Geophysical Research Letters, 25, 575–578.

Christian, J.W., and Vítek, V. (1970) Dislocations and stacking faults. Reports on Progress in Physics, 33, 307–411.

Davies, G.F. (1995) Penetration of plates and plumes through the mantle transition zone. Earth and Planetary Science Letters, 133, 507–516.

Denoual, C. (2007) Modeling dislocation by coupling Peierls-Nabarro and element-free Galerkin methods. Computer Methods in Applied Mechanics and Engineering, 196, 1915–1923.

Dorn, J.E., and Rajnak, S. (1964) Nucleation of kink pairs and the Peierls' mechanism of plastic deformation. Transactions of the Metallurgical Society of AIME, 230, 1052–1064.

Douin, J. (1987) Structure fine des dislocations et plasticité dans Ni_3Al. Ph.D. thesis, University of Poitiers, France (in French).

Dupas, C., Doukhan, N., Doukhan, J.C., Green, H.W. II, and Young, T.E. (1994) Analytical electron microscopy of a synthetic peridotite experimentally deformed in the β olivine stability field. Journal of Geophysical Research, 99, 15821–15832.

Dupas-Bruzek, C., Sharp. T., Rubie, D., and Durham, W. (1998) Mechanisms of transformation and deformation in $Mg_{1.8}Fe_{0.2}SiO_4$ olivine and wadsleyite under non-hydrostatic stress. Physics of the Earth and Planetary Interiors, 108, 33–48.

Farla, R., Amulele, G., Girard, J., Miyajima, N., and Karato, S.-I. (2015) High-pressure and high-temperature deformation experiments on polycrystalline wadsleyite using the rotational Drickamer apparatus. Physics and Chemistry of Minerals, 42, 541–558.

Fukao, Y., and Obayashi, M. (2013) Subducted slabs stagnant above, penetrating through, and trapped below the 660 km discontinuity. Journal of Geophysical Research: Solid Earth, 118, 5920–5938.

Fukao, Y., Widiyantoro, S., and Obayashi, M. (2001) Stagnant slabs in the upper and lower mantle transition region. Reviews of Geophysics, 39, 291–323.

Goldschmidt, V.M. (1931) Zur Kristallchemie des germaniums. Nachrichten von der Gesellschaft der Wissenschaften zu Göttingen, Mathematisch-Physikalische Klasse 1931, 184–190 (in German).

Grand, S.P. (2002) Mantle shear-wave tomography and the fate of subducted slabs. Philosophical Transactions: Mathematical, Physical and Engineering Sciences, 360, 2475–2491.

Grand, S.P., van der Hilst, R.D., and Widiyantoro, S. (1997) Global seismic tomography: A snapshot of convection in the Earth. Geological Society of America Today, 7, 1–7.

Guyot, P., and Dorn, J.E. (1967) A critical review of the Peierls mechanism. Canadian Journal of Physics, 45, 983–1016.

Huang, X., Xu, Y., and Karato, S.-I. (2005) Water content in the transition zone from electrical conductivity of wadsleyite and ringwoodite. Nature, 434, 746–749.

Hustoft, J., Amulele, G., Ando, J.-I., Otsuka, K., Du, Z., Jing, Z., and Karato, S.-I. (2013) Plastic deformation experiments to high strain on mantle transition zone minerals wadsleyite and ringwoodite in the rotational Drickamer apparatus. Earth and Planetary Science Letters, 361, 7–15.

Irifune, T., and Ringwood, A.E. (1987) Phase transformations in primitive MORB and pyrolite compositions to 25 GPa and some geophysical implications. In M.H. Manghnani and Y. Syono, Eds., High-Pressure Research in Mineral Physics, p. 231–242. American Geophysical Union, Washington, D.C.

Joós, B., Ben, Q., and Duesbery, M.S. (1994) Peierls-Nabarro model of dislocations in silicon with generalized stacking-fault restoring forces. Physical Review B, 50, 5890–5898.

Kárason, H., and van der Hilst, R.D. (2000) Constraints on mantle convection from seismic tomography. In M.R. Richards, R. Gordon, and R.D. van der Hilst, Eds., The History and Dynamics of Global Plate Motion, Geophysical Monograph, 121, 277–288. American Geophysical Union, Washington, D.C.

Karato, S.-I., Reidel, M.R., and Yuen, D.A. (2001) Rheological structure and deformation of subducted slabs in the mantle transition zone: Implications for mantle circulation and deep earthquakes. Physics of the Earth and Planetary Interiors, 127, 83–108.

Kawazoe, T., Karato, S.-I., Ando, J., Jing, Z., Otsuka, K., and Hustoft, J.W. (2010) Shear deformation of polycrystalline wadsleyite up to 2100 K at 14–17 GPa using a rotational Drickamer apparatus (RDA). Journal of Geophysical Research, 115, 1–11.

Kawazoe, T., Ohuchi, T., Nishihara, Y., Nishiyama, N., Fujino, K., and Irifune, T. (2013) Seismic anisotropy in the mantle transition zone induced by shear deformation of wadsleyite. Physics of the Earth and Planetary Interiors, 216, 91–98.

Kocks, U.F., Argon, A.S., and Ashby, M.F. (1975) Thermodynamics and Kinetics of Slip. Pergamon Press, New York.

Koizumi, H., Kirchner, H.O.K., and Suzuki, T. (1993) Kink pair nucleation and critical shear stress. Acta Metallurgica et Materialia, 41, 3483–3493.

——— (1994) Nucleation of trapezoidal kink pairs on a Peierls potential. Phillosophical Magazine A, 69, 805–820.

Kubin, L.P. (2013) Dislocations, mesoscale simulations and plastic flow. Oxford

University Press, U.K.
Metsue, A., Carrez, Ph., Denoual, C., Mainprice, D., and Cordier, P. (2010) Plastic deformation of wadsleyite: IV Dislocation core modelling based on the Peierls-Nabarro-Galerkin model. Acta Materialia, 58, 14671478.
Mitchell, T.E., Anderson, P.M., Baskes, M.I., Chen, S.P., Hoagland, R.G., and Misra, A. (2003) Nucleation of kink-pairs on partial dislocations: A new model for solution hardening and softening. Philosophical Magazine, 83, 1329–1346.
Mitrovica, J.X., and Forte, A.M. (2004) A new inference of mantle viscosity based upon joint inversion of convection and glacial isostatic adjustment data. Earth and Planetary Science Letters, 225, 177–189.
Möller, H.-J. (1978) The movement of dissociated dislocations in the diamond-cubic structure. Acta Metallurgica, 26, 963–973.
Nabarro, F.R.N. (1947) Dislocations in a simple cubic lattice. Proceedings of the Physical Society, 59, 256–272.
Nishihara, Y., Tinker, D., Kawazoe, T., Xu, Y., Jing, Z., Matsukage, K.N., and Karato, S.-I. (2008) Plastic deformation of wadsleyite and olivine at high-pressure and high-temperature using a rotational Drickamer apparatus (RDA). Physics of the Earth and Planetary Interiors, 170, 156–169.
Peierls, R.E. (1940) The size of a dislocation. Proceedings of the Physical Society, 52, 34–37.
Ringwood, A.E., and Major, A. (1966) Synthesis of Mg_2SiO_4-Fe_2SiO_4 spinel solid solutions. Earth and Planetary Science Letters, 1, 241–245.
Ritterbex, S., Carrez, Ph., Gouriet, K., and Cordier, P. (2015) Modeling dislocation glide in Mg_2SiO_4 ringwoodite: Towards rheology under transition zone conditions. Physics of the Earth and Planetary Interiors, 248, 20–29.
Sharp, T., Bussod, G., and Katsura, T. (1994) Microstructures in β-$Mg_{1.8}$ $Fe_{0.2}$ SiO_4 experimentally deformed at transition-zone conditions. Physics of the Earth and Planetary Interiors, 86, 69–83.
Tajima, F., and Grand, S.P. (1995) Evidence of high velocity anomalies in the transition zone associated with southern Kurile subduction zone. Geophycial Research Letters, 22, 3139–3142.
Takeuchi, S. (1995) Glide of interacting partial dislocations in the Peierls mechanism. Philosophical Magazine A, 71, 1255–1263.
Thurel, E. (2001) Etude par microscopie électronique en transmission des mécanismes de déformation de la wadsleyite et de la ringwoodite. Ph.D. thesis, University Lille 1 Science and Technology, France (in French).
Thurel, E., and Cordier, P. (2003) Plastic deformation of wadsleyite: I High-pressure deformation in compression. Physics and Chemistry of Minerals, 30, 256–266.
Thurel, E., Cordier, P., Frost, D., and Karato, S.-I. (2003a) Plastic deformation of wadsleyite: II High-pressure deformation in shear. Physics and Chemistry of Minerals, 30, 267–270.
Thurel, E., Douin, J., and Cordier, P. (2003b) Plastic deformation of wadsleyite: III. Interpretation of dislocations and slip systems. Physics and Chemistry of Minerals, 30, 271–279.
van der Hilst, R.D., Engdahl, R., Spakman, W., and Nolet, G. (1991) Tomographic imaging of subducted lithosphere below northwest Pacific island arcs. Nature, 353, 37–43.
van der Hilst, R.D., Widyantoro, S., and Engdahl, E.R. (1997) Evidence for deep mantle circulation from global tomography. Nature, 386, 578–584.
Wang, S-F. (2006) Dislocation energy and Peierls stress: A rigorous calculation from lattice theory. Chinese Physical Society, 15, 1301–1309.
Zhao, D. (2004) Global tomographic images of manlte plumes and subducting slabs: Insight into deep Earth dynamics. Physics of the Earth and Planetary Interiors, 146, 3–34.

Manuscript received October 5, 2015
Manuscript accepted March 27, 2016
Manuscript handled by Bijaya Karki